Computational and Structural Biotechnology Journal 21 (2023) 5144–5152

Contents lists available at ScienceDirect

Computational and Structural Biotechnology Journal

journal homepage: www.elsevier.com/locate/csbj

Research article

Computer-assisted stabilization of fibroblast growth factor FGF-18

Jan Vilim [a,b], Tereza Ghazalova [b], Eliska Petulova [b], Aneta Horackova [b], Veronika Stepankova [b], Radka Chaloupkova [b], David Bednar [a,c], Jiri Damborsky [a,c], Zbynek Prokop [a,c,*]

[a] Loschmidt Laboratories, Department of Experimental Biology and RECETOX, Faculty of Science, Masaryk University, Kamenice 5, 625 00 Brno, Czech Republic
[b] Enantis Ltd., INBIT, Kamenice 34, 625 00 Brno, Czech Republic
[c] International Clinical Research Center, St. Anne's University Hospital Brno, Pekarska 53, 656 91 Brno, Czech Republic

ARTICLE INFO

Keywords:
Computer-assisted stabilization
Fibroblast growth factor
Thermostability
Resistance to
Protease
Improved yield
FGF-18

ABSTRACT

The fibroblast growth factors (FGF) family holds significant potential for addressing chronic diseases. Specifically, recombinant FGF18 shows promise in treating osteoarthritis by stimulating cartilage formation. However, recent phase 2 clinical trial results of sprifermin (recombinant FGF18) indicate insufficient efficacy. Leveraging our expertise in rational protein engineering, we conducted a study to enhance the stability of FGF18. As a result, we obtained a stabilized variant called FGF18-E4, which exhibited improved stability with 16 °C higher melting temperature, resistance to trypsin and a 2.5-fold increase in production yields. Moreover, the FGF18-E4 maintained mitogenic activity after 1-week incubation at 37 °C and 1-day at 50 °C. Additionally, the inserted mutations did not affect its binding to the fibroblast growth factor receptors, making FGF18-E4 a promising candidate for advancing FGF-based osteoarthritis treatment.

1. Introduction

Growth factors (GFs) are small proteins influencing cellular processes by transducing signals leading to proliferation, differentiation or apoptosis. Fibroblast growth factors (FGFs) constitute an important GF family that can act in endocrine, paracrine, and intracellular fashion and influence cellular processes throughout cell life. Therefore, the roles of FGFs have been extensively studied in recent years [1–4]. Interestingly, the FGFs play a crucial role in many developmental processes; therefore, they are also implicated in the onset of diseases and their treatment [5].

From the practical perspective, the members that recently attracted the most attention years are fibroblast growth factor 2 (FGF2, also known as a basic fibroblast growth factor), fibroblast growth factor 7 (FGF7, also known as a keratinocyte growth factor) and FGF18. These FGF family members are implicated in wound regeneration (FGF2 and FGF7) and cartilage repair (FGF18) [3], respectively. Therefore, the current growing interest in regenerative medicine has resulted in the initiation of various clinical trials using FGF family members, albeit with limited success. Currently, the only FDA-approved drug derived from FGFs is palifermin, a truncated version of FGF7 used to treat oral mucositis resulting from radiotherapy [2,6].

The interest in FGF18 was sparked by its ability to stimulate bone formation [3,7], specifically, FGF18 is involved in chondrocyte proliferation and differentiation due to the interaction with fibroblast growth factor receptors (FGFRs) in proliferating chondrocytes and it also contributes to osteogenesis in periosteum/perichondrium [7]. The FGF18/fibroblast growth factor receptor (FGFR) interaction leads to the activation of MAPK/ERK pathway, which results in expression of Runx2 transcription factor and subsequently activation of genes related to bone formation [8,9]. Additionally, it has also been linked to the PI3K-AKT signaling with respect to the treatment of osteoarthritis by means of improving mitochondrial function [10]. In order to utilize these natural processes, the recombinant human FGF18 has been under development by Merck as a sprifermin, a drug with the potential to act as a disease-modifying compound for the treatment of osteoarthritis (OA). The treatment of OA presents a significant opportunity since the current obesity epidemic that plagues the world promises to increase the number of OA patients in coming years [11,12]. However, the results of the phase 2 clinical trial of sprifermin do not provide substantial encouragement. Although the drug exhibited a general capacity to halt the progression of the disease and contributed to the formation of additional cartilage (0.05 mm of the new cartilage with 100 μg of sprifermin every six months), the clinical relevance of the observation remained inconclusive both during the FORWARD trial [13] as well as the previous

* Corresponding author at: Loschmidt Laboratories, Department of Experimental Biology and RECETOX, Faculty of Science, Masaryk University, Kamenice 5, 625 00 Brno, Czech Republic.
E-mail address: zbynek@chemi.muni.cz (Z. Prokop).

https://doi.org/10.1016/j.csbj.2023.10.009
Received 3 August 2023; Received in revised form 5 October 2023; Accepted 6 October 2023
Available online 9 October 2023

Phase 1 trials [14,15]. It is important to note that none of the aforementioned studies reported significant side effects and thus strengthened the promise of FGF18 for OA treatment.

We were intrigued by the series of results, as it aligns with our previous hypothesis that the instability of fibroblast growth factors (FGFs) can hinder their full therapeutic potential as FGFs often exhibit a short half-life in vivo and low thermostability [16]. These limitations can pose a significant challenge that must be overcome to increase the applicability of FGFs, as we demonstrated on fibroblast growth factor 2 (FGF2), wherein we successfully elevated its melting temperature (T_m) by more than 20 °C and extended the half-life in vitro by more than 40-fold [17] using our protein stabilization tool FireProt [18]. The case of FGF18 being a promising target was further strengthened by the in vivo study using rats. Specifically, the study revealed that intact FGF18 is only present in the joint for 4 days and it exhibits tendency to form aggregates as well as degradation products [19]. Even though initially we did not deem FGF18 significantly unstable [16], we have decided to improve FGF18 using FireProt workflow. In an ideal scenario, the campaign would lead to a more stable FGF18 variant with the potential to alter the progression of OA.

2. Materials and methods

2.1. Computational design

Potentially stabilizing mutations were identified using the FireProt workflow [18] that relies on the combination of force-field-based free energy prediction and evolutionary approach. The evolution-based approach was utilized using a human FGF18 sequence (UniProt ID O76093, numbering of human FGF18 is used throughout the study) as the query for PSI-BLAST [20] with threshold E-values of 10^{-10} and 10^{-15} for the initial BLAST search and inclusion of a sequence in the position-specific matrix, respectively. Sequences collected after three PSI-BLAST iterations were clustered by CD-HIT [21] at a 90% identity threshold. The resulting dataset was clustered with CLANS [22] using default parameters to remove close homologs. Sequences were then used for the construction of multiple sequence alignment (MSA) with MUSCLE [23]. Back-to-consensus analysis was used on positions conserved in the MSA but were not present in the designed sequence. Simple consensus was used in positions where the consensus residue is present in at least 50% of all analyzed sequences. Ratio consensus was used in positions where consensus residue frequency is 40% and is at least five times more frequent than the wild-type amino acid. For the energy-based approach, a corresponding X-ray structure of human FGF18 (PDB ID 4CJM) [24] at 2.7 Å resolution, containing residues 50–190, was used. Before the analysis, the X-ray structure was cleaned from ligands (water, ions). The first step relied on the free energy change calculation using FoldX empiric force field [25] with the ΔΔG cut-off lower than 0 kcal.mol^{-1} (−1 kcal.mol^{-1} for the strict selection criteria). BiuldModel module was used with the following setting: pH 7, 298 K, 0.050 M ion strength, five rounds. The next step entailed the calculation of ΔΔG using Rosetta [26] according to protocol 16 by Kellog and colleagues [27] with Talaris2014 force field using the lowest value from 50 rounds of prediction. The energy threshold was set again to 0 kcal mol^{-1} for potentially stabilizing mutation (−1 kcal.mol^{-1} for the strict selection criteria). ConSurf webserver [28] was used to calculate the conservation scores of individual residues based on the MSA constructed in the evolutionary approach. All the potentially stabilizing mutations exhibiting conservation scores higher than 8 (7 for strict selection criteria) were discarded. Additionally, all mutations that were located in the functionally important regions were also omitted from the final selection. All single-point mutations passing all these filters were considered as stabilizing, any potential antagonistic effect was not predicted.

2.2. Protein expression

The chemicals used in this study were purchased from Sigma-Aldrich unless stated otherwise. Genes coding FGF18-WT, FGF18-E1, FGF18-E2 and FGF18-F1 with N-terminal His-tag sequence and thrombin cleavage site (amino acid sequences are specified in Supplementary Table S1 and Supplementary alignment S2 for comparison of variants of the study to sprifermin; the numbering of the human FGF18 was used; the variants consist from 21 AA forming the His-tag and residues 28–207 of FGF18, UniProt ID O76093) were commercially synthesized (GeneArt), and the genes coding for FGF18-E3 and FGF18-E4 were prepared by site-directed mutagenesis using Q5-Directed mutagenesis Kit (New England Biolabs). All genes were cloned into pET28b plasmid (MerckMillipore) and transformed into an *Escherichia coli* NEB-5α strain (New England Biolabs). The plasmids were isolated, their sequence was verified, and they were subsequently cloned into *E. coli* BL21 DE3 (New England Biolabs). A single colony was used to inoculate a 50 mL starting overnight culture consisting of LB media and kanamycin (50 μg mL^{-1} final concentration). The starting culture was incubated overnight at 37 °C, 200 rpm. 25 mL of starting culture was used to inoculate the main culture (2 L total volume) with kanamycin (50 μg mL^{-1} final concentration). The main culture was incubated at 37 °C, 200 rpm (Multitron, HT Infors) until the OD600 reached the values of 0.6–0.8. The culture was subsequently cooled down (20 °C), the expression was induced with IPTG (0.5 mM final concentration) and the main culture was incubated overnight at 20 °C, 200 rpm in the same incubator as before. The resulting culture was subsequently centrifuged (ca 2500 g, 20 min, 4 °C; machine), re-suspended in loading buffer (20 mM K-phosphate buffer, 500 mM NaCl, 10 mM imidazole, pH 7.5) and stored at − 80 °C for further use.

2.3. Protein purification

The bacterial suspension in loading buffer (20 mM K-phosphate buffer, 500 mM NaCl, 10 mM imidazole, pH 7.5) was disintegrated using sonication (2 s on, 2 s off, 15 min, 100% amplitude; UP200S, Hielscher), and the sonicate was centrifuged (60 min, 20 000 g, 4 °C). The resulting supernatant was filtered through a 0.45 μm filter and purified on an AKTA FLPC system (GE Healthcare) using a cOmplete™ His-Tag Purification Column (Merck). The elution was performed using gradient elution with an elution buffer containing 300 mM imidazole. The obtained protein was further dialyzed overnight at 4 °C into the storage buffer (20 mM K-phosphate buffer, 500 mM NaCl, pH 7.5). The protein yield was determined using Pierce™ Coomassie Plus (Bradford) Assay Kit (Thermo Fisher Scientific). The resulting protein solution was diluted to 1 mg mL^{-1}, divided into 1 mL aliquots, lyophilized and stored for further use at − 80 °C.

2.4. Secondary structure

Circular dichroism (CD) spectra of mutants dialyzed in 50 mM phosphate buffer pH 7.5 and diluted to the concentration of 0.2 mg mL^{-1} were recorded at 20 °C using a spectropolarimeter Chirascan (Applied Photophysics) equipped with a Peltier thermostat. Data were collected from 200 to 260 nm, at 100 nm min^{-1}, 1 s response time, and 2 nm bandwidth using a 0.1 cm-quartz cuvette. Each spectrum is the average of five individual scans and is corrected for absorbance caused by the buffer. Collected CD data were expressed in terms of the mean residue ellipticity.

Additionally, the thermal unfolding was analyzed by monitoring the ellipticity at 227 nm over the temperature range from 20 to 80 °C at a heating rate of 1 °C min^{-1}. Recorded thermal denaturation curves of FGF18 variants were normalized to represent signal changes between approximately 0 and 1 and fitted to sigmoidal curves. The T_m values were evaluated from the collected data as a midpoint of the normalized thermal transition, using the OriginPro8 software.

2.5. Thermal stability

The thermostability of obtained variants was determined by differential scanning calorimetry (DSC). Thermal unfolding of 1.0 mg mL^{-1} protein solutions in 50 mM phosphate buffer (pH 7.5) with 750 mM NaCl was followed by monitoring the heat capacity using the VP-capillary DSC system (GE Healthcare). The measurements were performed at temperatures from 20 to 80 °C or from 20 to 100 °C at 1 °C min^{-1} heating rate. T_m was evaluated as the top of the Gaussian curve after the manual setting of the baseline.

2.6. Cell proliferation

The cell proliferation assay was performed as reported previously [29]. BaF3 cells expressing FGFR-2C [30] were maintained in DMEM medium (Biosera) with 10% newborn calf serum (NCS; Merck), 4 mM L-glutamine, 100 U mL^{-1} of penicillin, 100 μg mL^{-1} of streptomycin (i.e.,1 × Pen/Stre; all Thermo Fisher Scientific), 600 μg mL^{-1} G418, 50 μM β-mercaptoethanol (both Merck) and 0.5 ng mL^{-1} mouse interleukin 3 (IL3; Peprotech). For BaF3 proliferation assays, 4 × 10^4 cells per well were seeded in 96-well plates in BaF3 basal medium (with serum: 10% NCS, 1 × Pen/Strep in RPMI-1640; or serum-free: 0.05 × insulin-transferrin-selenium (ITS; Thermo Fisher Scientific), 1 × Pen/-Strep in RPMI-1640) with or without heparin (0–2 g mL^{-1}; Thermo Fisher Scientific), or with protamine sulfate (250 μg mL^{-1}; Thermo Fisher Scientific) as required for the experiments and incubated overnight at 37 °C, 5% CO_2. The next day the FGF18 variants at different concentrations (as needed for the experiment) were added to the plates. Within each experiment, all treatments were done in triplicates. The cells were incubated with FGF18 variants for 3 days. Subsequently, resazurin was added to the plate to the final concentration 10 μg mL^{-1} and the plates were incubated for 6–24 h (until resazurin color change was observed). The same incubation time was strictly adhered to for all plates within the same experiment. Resorufin fluorescence (excitation at 560 nm, emission at 590 nm) was measured using Synergy H4 Hybrid multi-mode microplate reader (BioTek). The resulting ED_{50} value corresponds to the amount of protein which results in 50% of the maximal cell count.

2.7. Protein aggregation

The aggregation during the purification workflow was measured using a Bradford assay using Pierce™ Coomassie Plus (Bradford) Assay Kit (Thermo Fisher Scientific). The protein samples before dialysis, after dialysis and after the reconstitution of lyophilized samples were measured according to the manufacturer's protocol.

The aggregation temperature (T_{agg}) was determined using the UNCLE reader (Unchained Labs). The protein was reconstituted in distilled water at the 1 mg mL^{-1} concentration, and the 9 μL of the sample was transferred into a micro-volume quartz cuvette (Unchained Labs). The T_{agg} was determined using the SLS program with a wavelength set at 266 nm over the temperature range between 15 and 95 °C. The rate of temperature change was 1 °C min^{-1}. The data were evaluated using the supplied software.

2.8. Proteolytic resistance

The proteolytic degradation of FGF18-WT (Peprotech) and FGF18-E4 was measured by their resistance to the degradation by trypsin. Freshly reconstituted protein samples were incubated with trypsin (1:20, trypsin:FGF18 variant ratio) for 240 min. The 10 μL aliquots were taken every 5 min until 30 min time-point and subsequently analyzed by SDS-PAGE and band densitometry. The half-life was calculated using a One-phase decay equation (Y=(Y0 - Plateau)*exp(-K*X) + Plateau) and the fitting was performed using a GraphPad Prism 9 software.

2.9. Activity retention

The investigation into the activity retention was performed in the same fashion as the cell proliferation assay using BaF3 cells expressing FGFR-2 C (described in paragraph *Cell proliferation*). In terms of the preparation for the protein sample, the lyophilized samples of commercially available FGF18-WT (Peprotech) and FGF18-E4 were reconstituted in distilled water, diluted to 100 μg mL^{-1} with 0.1% BSA solution and incubated at three different temperatures − 20 °C, 37 °C and 50 °C for 24 h, 7 days or 24 h, respectively. After the incubation, the protein samples were added to the 96-well plates containing the cells, and the experiment was performed as described above. The concentration of the FGF18 variant is expressed in molar concentration due to the difference in molecular weight of FGF18-E4 and Commercially available FGF18-WT. In order to visualize the change, the results were compared to the normalized growth curve obtained with freshly reconstituted protein.

2.10. Receptor specificity

The receptor specificity was determined using in-house prepared freshly reconstituted FGF18-E4 and commercially available freshly reconstituted FGF18-WT (Peprotech). The concentration of both proteins was verified, the proteins were diluted to 100 μg mL^{-1} with 0.1% BSA solution. The concentration of the FGF18 variant is expressed in molar concentration due to the difference in molecular weight of FGF18-E4 and commercially available FGF18-WT. The testing itself was performed in the same fashion as was described before in the *Cell Proliferation* paragraph. The BaF3 cells that were used to express different variants of FGFRs, namely both "B" and "C" isoforms of FGFR1, FGFR2 and FGFR3, respectively [30].

3. Results

3.1. Design and evaluation of the first generation of FGF18 variants

The energetic and evolutionary approach yielded 19 mutations at 12 distinct positions and 8 mutations at eight positions, respectively. Since we found it challenging to produce FGF18 in soluble form (see Supplementary Table S3), we have opted to construct directly multiple-point mutants. The three variants were designed following different criteria for selection of the mutations: i) strict selection criteria $\Delta\Delta G < -1$ for both FoldX and Rosetta, conservation analysis value < 8 and intact salt bridges resulted in FGF18-E1 variant, ii) less strict criteria for $\Delta\Delta G < 0$, conservation analysis value < 9, intact salt bridge resulted in FGF18-E2 variant, and iii) consensus analysis using insertion of the consensus mutation to least conserved position with most consistent potential for stabilization resulted in FGF18-F1 variant (see Table 1 for a summary of identified mutations). The strict selection criteria led to a three-point mutant containing residues L141F, S147P and Q170P (FGF18-E1). These particular mutations provided the largest stabilization *in silico* using both FoldX and Rosetta. The second less-stringent set of criteria led to a seven-point mutant comprised of the three aforementioned residues plus R71P, R72Q, Q96F and V128W (FGF18-E2). This variant exhibited a high level of theoretical stabilization (< −1.800 kcal mol^{-1}), albeit only when the Rosetta was utilized. The back-to-consensus analysis revealed eight possible mutations, from which we chose four that led to the highest predicted stabilization.

The three variants were constructed, expressed, and characterized with a focus on evaluating the protein yield, melting temperature (T_m) and biological activity. Notably, all variants exhibited a significant increase in T_m value. Specifically, FGF18-E1 showed that the T_m increased by 10 °C using both CD and DSC measurements. FGF18-E2 and FGF18-F1 afforded the increase of T_m by 9 °C while using CD, which was confirmed by DSF analysis, with FGF18-E2 showing an 8 °C and FGF18-F1 6 °C increase in T_m. Regarding the biological activity, the FGF18-E1

Table 1
Single-point mutations designed by the FireProt protein stabilization platform based on force-field calculations and phylogenetic analysis used for the construction of the first generation of FGF18 variants.

Substitution	FoldX ΔΔG (kcal/mol)	Rosetta ΔΔG (kcal/mol)	Cons.	AA profile	AA frequency	Most frequent AA	Variant
Energy-based mutations							
R71F	-0.053	-1.868	5	N,P,K,G,Q,R,L	n.a.	n.a.	
R71M	-0.258	-0.403	5	N,P,K,G,Q,R,L	n.a.	n.a.	
R71P	-0.898	-1.834	5	N,P,K,G,Q,R,L	n.a.	n.a.	E2
R71W	-0.341	-2.842	5	N,P,K,G,Q,R,L	n.a.	n.a.	
R72Q	-0.040	-2.639	5	Y,S,R,D,P,T,A,N,K	n.a.	n.a.	E2
S74F	-0.067	-1.231	5	M,T,N,K,G,S,V,L,R,D	n.a.	n.a.	
Y83F	-0.365	-0.039	6	H,Y,F,N	n.a.	n.a.	
Q85W	-0.235	-2.799	7	E,Q,R,L,S,K,N,T	n.a.	n.a.	
Q96F	-0.719	-2.005	7	H,Q,R,K	n.a.	n.a.	E2
Q96Y	-0.283	-2.401	7	H,Q,R,K	n.a.	n.a.	
T104V	-0.093	-0.174	8	P,T,S	n.a.	n.a.	
V128I	-0.067	-0.483	5	A,M,T,F,I,L,Q,Y,V	n.a.	n.a.	
V128W	-0.028	-3.044	5	A,M,T,F,I,L,Q,Y,V	n.a.	n.a.	E2
L141F	-1.431	-3.087	7	F,Y,L,W,H	n.a.	n.a.	E1, E2
L141Y	-1.537	-2.159	7	F,Y,L,W,H	n.a.	n.a.	
S147P	-1.819	-2.191	1	T,A,N,K,G,V,S,L,R,D,E,P	n.a.	n.a.	E1, E2
S147Y	-1.100	-1.152	1	T,A,N,K,G,V,S,L,R,D,E,P	n.a.	n.a.	
R166S	-0.411	-1.064	5	I,H,Q,L,R,S,G,K,A,T	n.a.	n.a.	
Q170P	-1.944	-1.750	7	E,K,N,R,Q,G	n.a.	n.a.	E1, E2
Evolution-based mutations							
I66V	0.847	-0.692	n.a.	n.a.	0.23	0.61	
Q85K	0.012	0.460	n.a.	n.a.	0.16	0.55	F1
Q96R	-0.119	-0.394	n.a.	n.a.	0.23	0.52	F1
L108I	0.262	1.193	n.a.	n.a.	0.42	0.52	
R112K	-0.017	-1.194	n.a.	n.a.	0.26	0.55	F1
K113R	0.283	0.706	n.a.	n.a.	0.29	0.58	F1
K196R	n.d.	n.d.	n.a.	n.a.	0.32	0.61	
R199K	n.d.	n.d.	n.a.	n.a.	0.32	0.61	

n.a. – not applicable – for mutations where the value was not used for selection; n.d. – not determined due to missing structure; Cons. – Conservation of the WT residue determined by ConSurf web server; AA – amino acid.

exhibited comparable ED_{50} values to the wild-type, while FGF18-E2 exhibited a slight increase. It is important to note that a lower ED_{50} value indicates higher activity or stability, as it requires a smaller amount of protein to produce the same effect, particularly concerning cellular proliferation. The determination of the ED_{50} value for FGF18-F1 was impeded due to its tendency to precipitate upon addition to the cellular culture. Additionally, we evaluated the protein yield obtained from a liter of culture medium. Based on a thorough analysis of the obtained results (Table 2), we have chosen FGF18-E1 as the base variant for the second engineering phase.

Table 2
Comparison of stability, yield and biological activity of FGF18-WT and the first generation of stable FGF18 variants. Error values for CD – denote the expected imprecision of the Boltzmann curve fit. Error values for DSF – represent standard deviation determined from three measurements.

Protein variant	Mutations	Yield [mg L^{-1}]	Biological activity ED_{50} [ng mL^{-1}]	Melting temperature T_m [°C]	
				CD	DSF
FGF18-WT	n.a.	5	4	47.3 ± 0.6	43.3 ± 0.1
FGF18-E1	L141F; S147P; Q170P	6	5	57.0 ± 0.2	52.8 ± 0.1
FGF18-E2	R71P; R72Q; Q96F; V128W; L141F; S147P; Q170P	10	18	56.4 ± 0.2	50.8 ± 0.1
FGF18-F1	Q85K; Q96K; R112K; K113R	5	n.d.	56.4 ± 0.2	48.8 ± 0.1

n.a. – not applicable; ED_{50} – efficient dosage for 50% of observed effect; n.d. – not determined due to aggregation; CD – circular dichroism; DSF – differential scanning fluorimetry.

3.2. Design and evaluation of the second generation of FGF-18 variants

FGF18-E1 was taken as a template for the *in silico* identification of stabilizing mutations leading to the second generation of the stable FGF18 molecule. Only the energy-based approach was utilized since the evolution-based approach would not provide new mutations. This additional *in silico* analysis identified five mutations occurring at five distinct positions (Table 3). Following the application of the strict selection criteria, two mutations, namely Q85W and E105G, remained for further analysis. We have decided to construct two mutant variants. The first, a four-point mutant, denoted as FGF18-E3, incorporating the E105G mutation into FGF18-E1. The second variant is a five-point mutant, designated as FGF18-E4, incorporating both eligible mutations (E105G and Q85W) into FGF18-E1.

The second-generation variants were expressed, purified and subjected to identical analysis as the first-generation variants. To our

Table 3
Single-point mutations afforded by force-field calculations.

Substitution (FGF18-E1)	FoldX ΔΔG (kcal mol^{-1})	Rosetta ΔΔG (kcal mol^{-1})	Cons.	AA profile	Variant
Q85W	-2.537	-1.041	6	L,S,Q,E,K,R,T	E4
S95Y	-1.770	-0.495	6	G,M,S,A,K,R,H	
Q96Y	-2.004	0.236	6	Q,H,R,K	
E105G	-1.911	-2.080	2	K,G,P,D,Q,S,R,N,E,A	E3, E4
V117F	-2.191	1.229	5	M,V,K,H,I,L,R,T	

Cons. – Conservation of the WT residue determined by ConSurf web server; AA – amino acid.

delight, both variants exhibited an additional increase in T_m confirmed by both analytical methods. CD spectrometry revealed that FGF18-E3 and FGF4-E4 exhibit an increase of T_m by 18 and 16 °C, respectively, compared to the wild type. DSF measurement corroborated the findings, with the ΔT_m values of 15 °C and 16 °C provided for FGF18-E3 and FGF4-E4, respectively (Table 4). Moreover, both variants afforded higher production yield than the FGF18-WT. Notable improvement was observed in the case of FGF18-E4, where the yield was doubled. Furthermore, we have observed the same (FGF18-E3, 4 ng mL^{-1}) or slightly increased (FGF18-E4, 1 ng mL^{-1}) ED_{50} values for both multiple-point variants. The five-point mutant FGF18-E4 was selected for further testing and comparison with FGF18-WT.

3.3. Comparison of FGF18-E4 with FGF18-WT

We compared the operational stability of FGF18-WT (wild-type) and the most stable variant FGF18-E4 by monitoring the aggregation throughout the production process. Specifically, we assessed protein loss due to aggregation during affinity chromatography purification, dialysis into the storage buffer, and lyophilization before long-term storage. The protein yield was evaluated from a liter of culture before and after dialysis, which showed that the FGF18-E4 had an elevated ability to withstand dialysis conditions. Furthermore, FGF18-E4 also exhibited significantly lower losses than the progenitor molecule after reconstitution of the lyophilized sample. Specifically, the loss during reconstitution was 5% of the pre-lyophilization concentration in the case of FGF18-E4 compared to a 35% loss in the case of FGF18-WT. Together with the 20% higher overall yield, these improvements resulted in a 2.5-fold increase in the total amount of protein that was obtained from 1 L of culture (Fig. 1a).

Additionally, we have decided to corroborate the lowered aggregation propensity of FGF18-E4 further using SLS to determine the aggregation temperature (T_{agg}, Fig. 1b). The analysis demonstrated a clear difference between the FGF18-WT and the FGF18-E4. More specifically, the FGF18-WT started aggregating at 39.3 °C, whereas the FGF18-E4 started aggregating at the temperature of 53.0 °C, which further confirms the increased general stability of this variant, including resistance to aggregation processes.

The comparison of proteolytic resistance of the FGF18-WT and FGF18-E4 to the trypsin was performed in K-Phosphate buffer (20 mM, 500 mM NaCl, pH 7.5) in the presence of 0.05 equivalents of trypsin as a model protease. Using the online tool PeptideCutter [31] to detect cleavage sites (see Supplementary analysis S4), we identified 36 potential trypsin cleavage sites for FGF18-WT and FGF18-E4. The protein cleavage was monitored for 240 min using SDS-PAGE (Fig. 2a) followed by densitometric analysis of resulting protein bands (Fig. 2b).

Table 4
Comparison of stability, yield and biological activity of FGF18-WT and the second generation of engineered FGF18 variants. Error values for CD – denote the expected imprecision of the Boltzmann curve fit. Error values for DSF – represent standard deviation determined from three measurements.

Protein variant*	Mutations	Yield [mg L^{-1}]	Biological activity ED_{50} [ng mL^{-1}]	Melting temperature T_m [°C]	
				CD	DSF
FGF18-WT	n.a.	5	4	47.3 ± 0.6	43.3 ± 0.1
FGF18-E3	L141F; S147P; Q170P; E105G	6	4	65.2 ± 0.3	58.2 ± 0.1
FGF18-E4	L141F; S147P; Q170P; E105G; Q85W	10	1	62.8 ± 0.2	58.8 ± 0.3

n.a. – not applicable; ED_{50} – efficient dosage for 50% of observed effect; n.d. – not determined; CD – circular dichroism; DSF – differential scanning fluorimetry.

Interestingly, the FGF18-E4 exhibited 16-fold increased proteolytic resistance, with FGF18-WT and FGF18-E4 having a half-life of 11.8 and 193.2 min, respectively. We assume this result is caused by the increased general stability of FGF18-E4 since the number of cleavage sites in our final variant did not change compared to the parent molecule.

The mitogenic activity of FGF18-E4 and FGF18-WT was studied at three different temperatures, − 20 °C, 37 °C and 50 °C and further compared to a reference experiment using the BaF3 cell line expressing the FGFR-2C receptor. FGF18-E4 exhibited superior proliferative activity compared to FGF18-WT in all three conditions (Fig. 3). The FGF18-E4 retained its mitogenic activity almost fully after 1 week of incubation at 37 °C (Fig. 3b) and to a lesser degree after 24 h at − 20 °C (Fig. 3a) and at 50 °C (Fig. 3c). Interestingly, this suggests that the freeze-thawing cycle is less favorable for FGF18-E4 compared to prolonged incubation at 37 °C. It also shows the rapid drop of activity of FGF18-WT in all three conditions.

The receptor specificity of FGF18-E4 was assessed using BaF3 cells expressing different variants of fibroblast growth factor receptors (FGFRs 1B, 1C, 2B, 2C, 3B, and 3C) and compared to commercially available FGF18-WT (Peprotech). The results, as shown in Fig. 4, indicate that the introduction of stabilizing mutations did not alter the receptor specificity. Specifically, we observed a similar proliferation induction profile to FGF18-WT. The lines expressing receptor variants FGFR-2C and FGFR-3C demonstrated proliferation induction (Figs. 4e and 4f, respectively), while the cell lines overexpressing remaining receptor isoforms exhibited negligible or no growth in the presence of both FGF18-WT and FGF18-E4 (Figs. 4a-4d). The experiment revealed a similar activity profile between the original molecule and the engineered variant.

4. Discussion

Here, we have focused on improving a clinically relevant growth factor FGF18 [5] potentially suffering from insufficient operational stability [16]. We have employed a FireProt workflow previously successfully utilized to enhance the stability of FGF2 [17]. As opposed to the FGF2 campaign, this project commenced with the construction of multiple-point variants directly. This alteration stemmed from the initial difficulty in expressing the FGF18-WT in a soluble form. By applying stringent selection criteria, three multiple-point variants were obtained during the initial round of mutagenesis. The characterization of the variants led to the identification of a template with significantly enhanced stability FGF18-E1. This finding highlights the potential of employing curated stabilizing mutations generated through FireProt, reducing the experimental workload by focusing on the expression and characterization of three multiple-point variants instead of 7–12 single-point variants and subsequent combinations of the most stabilizing ones.

The second round of *in silico* analysis following the same workflow ultimately afforded variant FGF18-E4. This variant comprising five mutations (Q85W, E105G, L141F, S147P, and Q170P) demonstrated the potential of the workflow to improve unstable molecules iteratively since one of the two potentially stabilizing mutations identified during the second round of *in silico* analysis (E105G) was not part of the initial set. It shows the importance of iteration of calculations to address the changes introduced by the initial mutations. With each iteration, fewer mutations and lower stabilizing effects can be expected, as was recently shown on the stabilization of haloalkane dehalogenase [32].

The final variant, FGF18-E4, exhibits significantly enhanced operational parameters. Introducing five mutations increased an apparent T_m of the FGF18-WT by 16 °C. Additionally, the significant lowering of the aggregation during the production process led to an approximately 2-fold increase in observed yield and 4-fold yield after the reconstitution of lyophilized protein and the reduced propensity to aggregate when exposed to elevated temperatures. Moreover, we have demonstrated that the FGF18-E4 is 16-fold less susceptible to proteolytic degradation,

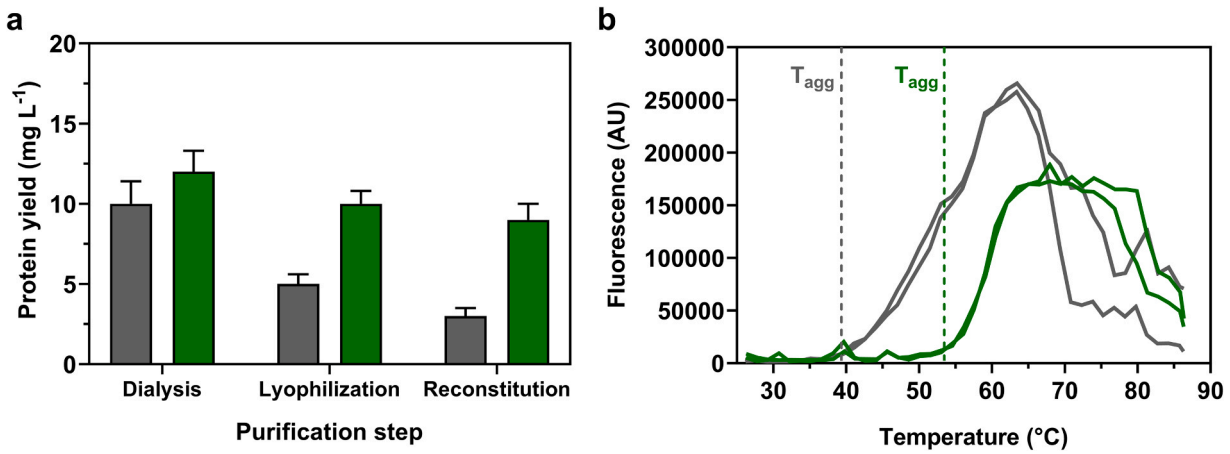

Fig. 1. The aggregation propensity of FGF18-WT (grey) and FGF18-E4 (green). a) Comparison of aggregation-mediated losses of FGF18 variants during purification; The error bars represent standard deviation (n = 3). b) Aggregation analysis from two independent runs of each variant with highlighted temperature-induced aggregation (T_{agg}, dashed line). The analysis was performed using reconstituted protein in 20 mM K-phosphate buffer at pH 7.5 containing 500 mM NaCl according to the procedure listed in the Materials and methods.

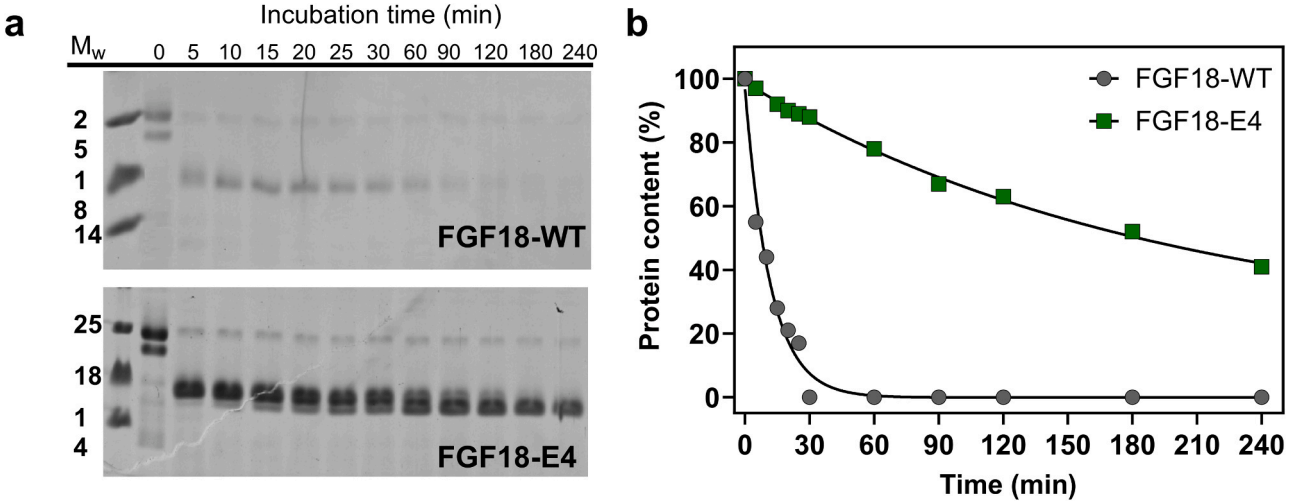

Fig. 2. Comparison of proteolytic stability of FGF18-WT and FGF18-E4 upon incubation with trypsin. a) SDS-PAGE visualization of remaining FGF18 variants; b) Results of densitometric analysis of a gel from section a, FGF18-WT is depicted in grey and FGF18-E4 in green. The analysis was performed using reconstituted FGF18-WT and FGF18-E4 in 20 mM K-phosphate buffer at pH 7.5 containing 500 mM NaCl. The FGF18 variants were incubated with 0.05 mol equivalents of trypsin according to the procedure listed in the Materials and Methods.

and it can withstand a one-week incubation at 37 °C without a significant drop in the ability to induce proliferation. Additionally, we have shown that the freeze-thaw cycle significantly decreases the performance of FGF18-WT. On the other hand, the performance of FGF18-E4 was very similar to the reference experiment, especially in the higher concentrations of FGF18-E4 (1 and 10 nM).

We have actively tried to avoid introducing mutations into the regions of FGF18 that were implicated in the binding to the FGFRs, especially to the residues located in the hydrophobic binding region [24]. Interestingly, the initial analysis of FGF18 binding was performed by superpositioning FGF18 molecule on the FGF8 molecule bound to FGFR-2C in the same contribution. The same superposition of the FGF18-E4 (FGF18-E4 atop of FGF8-FGFR2C complex) revealed that only the residue Q170P is located near the ligand-receptor interface (see Supplementary analysis S5). The negligible effect of the introduced mutations on the receptor interaction is further corroborated by the matching receptor specificity of FGF18-WT and FGF18-E4, as far as we can infer from the results of cell proliferation assays with BaF3 cells expressing different isoforms of FGFRs. In detail, we have observed the induction of proliferation in BaF3 cells expressing FGFR-2C and FGFR-3C, both with FGF18-WT and FGF18-E4, which has been described previously for FGF18-WT [33]. We have to mention that the literature reports the interaction between FGF18 and FGFR-3B as well, however, we were not able to detect that using our proliferation-based assay.

The stability improvements presented in this study gain further significance when the performance of sprifermin in the last clinical trials is investigated. Over the last decade, sprifermin has positively affected connective tissue regeneration in several contributions, such as the *ex vivo* bovine cartilage [34,35] or the torn rat rotator cuff repair model [36]. Its mode of action has been linked to signaling by extracellular signal-regulated kinases [37]. However, the performance of sprifermin in clinical trials has been less impressive. One Phase 1 clinical trial failed to meet its primary target - reduction of a cartilage loss in the central medial femorotibial compartment, albeit there were positive effects on the femerotibial joint as well as the lateral femorotibial compartment [14] and no negative effects stemming from systemic exposure were detected in another [15]. Moreover, the recent results of the Phase 2 FORWARD study did not provide clear evidence of clinically relevant improvement [13]. More specifically, the 100 μg dose given every 6 or

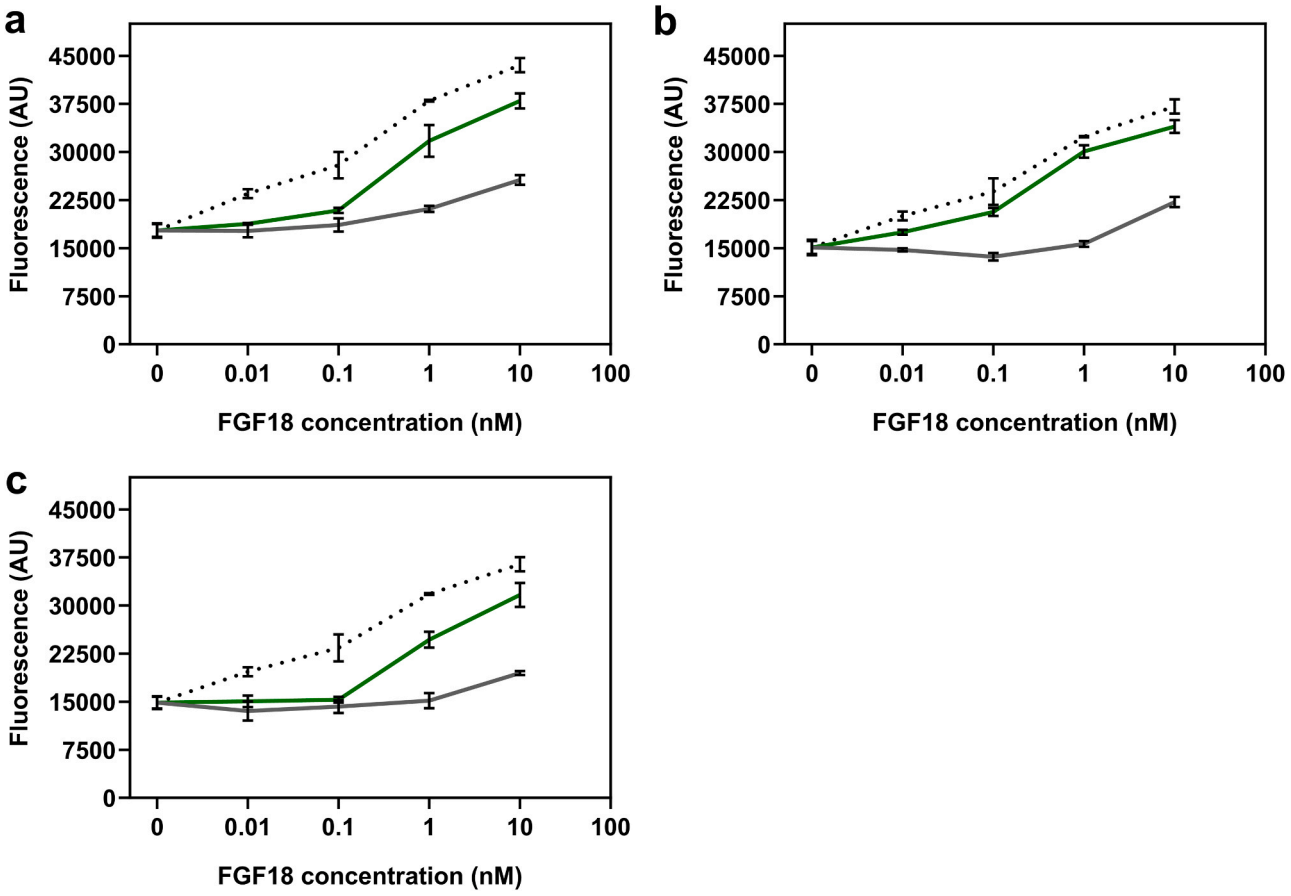

Fig. 3. Comparison of the ability of FGF18-WT (grey) and FGF18-E4 (green) to induce proliferation after incubation at different temperatures with respect to a normalized performance of a fresh FGF18-WT. a) 24 h incubation at − 20 °C; b) 7 days incubation at 37 °C; c) 24 h incubation at 50 °C. The error bars represent the standard deviation (n = 3). The FGF18-WT and FGF18-M4 were incubated in 20 mM K-phosphate buffer at pH 7.5, containing 500 mM NaCl. The proliferation assay was run over the course of 4 days and the proliferation was evaluated via resazurin assay as described in the Materials and methods.

12 months over 24 months resulted in a statistically significant increase in cartilage thickness. In detail, 6 and 12-month regimens resulted in 0.05 mm and 0.03 mm of new cartilage, respectively, whereas the increases in cartilage thickness using 30 μg doses given in the same intervals resulted in statistically insignificant improvements. Interestingly, it seems that the cartilage gained due to the sprifermin treatment possesses the same characteristics as the native cartilage, suggesting that the treatment will have a lasting effect [38].

The results above indicate that the sprifermin treatment holds great potential. We expect that the instability of FGF18-WT that we observed is a contributing factor for the underwhelming performance of the sprifermin since we have demonstrated the low ability of FGF18-WT to induce proliferation of BaF3 cells after the incubation at 37 °C. This is a likely operating condition upon the injection into the knee joint and it has been determined in rats that sprifermin effectively disappears from the joint 4 days after intra-articular injection [19]. In contrast, the FGF18-E4 maintained the ability to induce proliferation after incubation at 37 °C for 1 week or even 50 °C for 1 day. The data describing the increased stability at 37 °C and the decreased aggregation propensity compared to FGF18-WT (53 °C vs. 39 °C) suggest a higher probability of a positive effect on the cartilage regeneration simply due to the longer exposure time. Therefore, the development of FGF18-E4 represents a first step towards FGF18-based osteoarthritis medicine with the potential to slow and revert the disease progression. In the following study, we will further focus on improving expressibility and operational stability and the application-related parameters, such as in vivo longevity of FGF18-E4.

5. Conclusions

The study aimed to enhance the stability of a growth factor FGF18 by utilizing a FireProt workflow combining force-field calculations and phylogenetic analysis. In the initial phase of the stabilization design, we successfully obtained three variants of FGF18. Among these variants, FGF18-E1 emerged as the most promising, demonstrating the highest level of stabilization. Consequently, FGF18-E1 underwent a second round of engineering, ultimately developing the final variant, FGF18-E4. This variant showed outstanding thermal and operational stability improvement, effectively minimized aggregation and reduced susceptibility to proteolytic degradation. Importantly, stabilizing mutations did not disrupt the receptor specificity of the engineered FGF18 variants. Even after exposure to elevated temperatures, the stable FGF18-E4 retained its proliferative ability, indicating its potential efficacy in promoting cartilage regeneration. The development of FGF18-E4 marks a significant advancement towards creating an FGF18-based medicine for osteoarthritis, holding promise in slowing down or even reversing the progression of the disease.

Declaration of Generative AI and AI-assisted technologies in the writing process

During the preparation of this work the authors used ChatGPT in order to improve language. After using this tool, the authors reviewed and edited the content as needed and take full responsibility for the content of the publication.

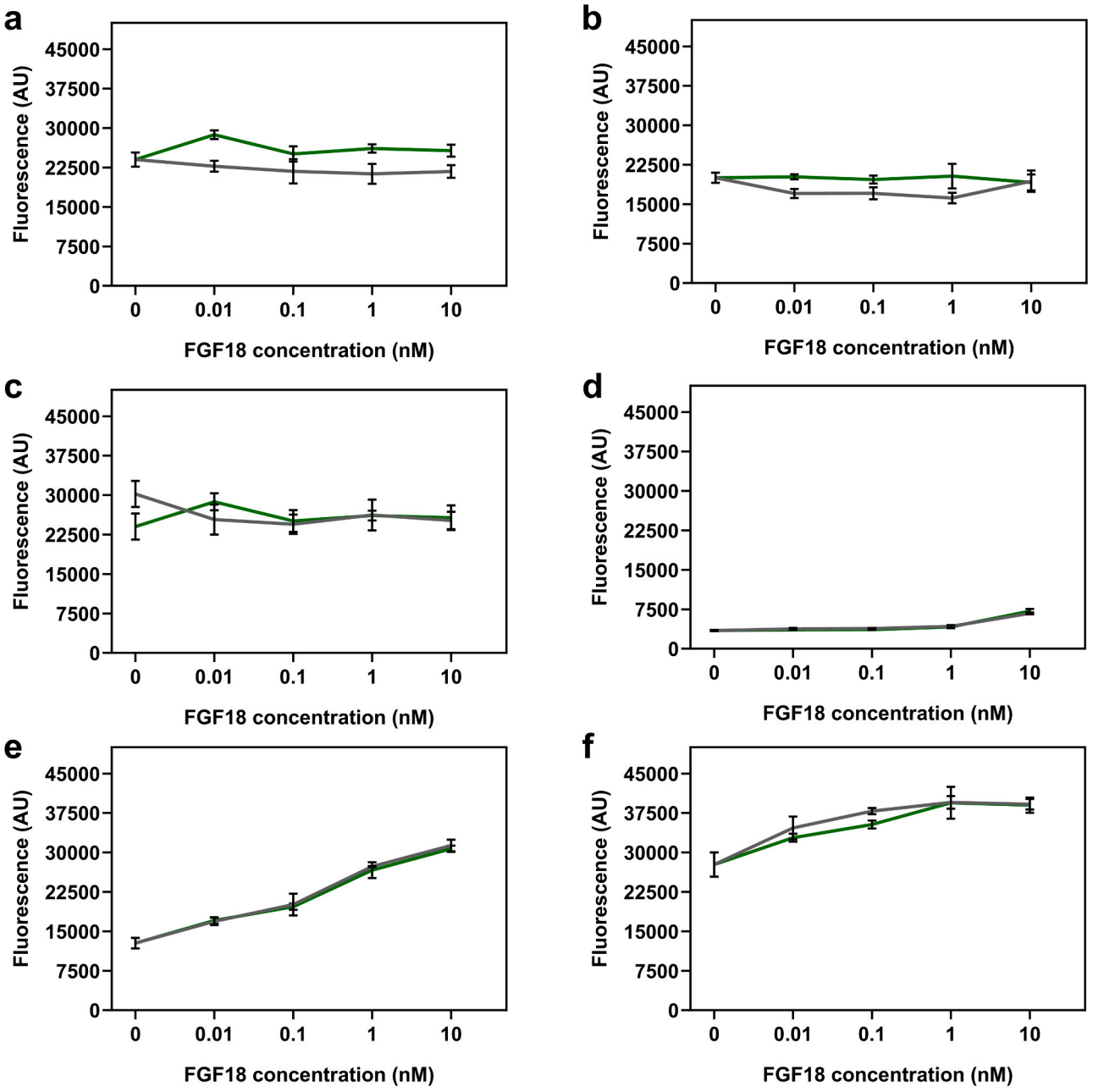

Fig. 4. Comparison of receptor specificity of FGF18-WT (grey) and FGF18-E4 (green) with different FGFRs. a) FGFR-1B; b) FGFR-2B; c) FGFR-3B; d) FGFR-1C; e) FGFR-2C; f) FGFR-3C. The error bars represent the standard deviation (n = 3). The FGF18-WT and FGF18-E4 were prepared in 20 mM K-phosphate buffer at pH 7.5, containing 500 mM NaCl containing 0.1% BSA. The proliferation assay was run over the course of 4 days and the proliferation was evaluated via resazurin assay as described in the Materials and methods.

Conflict of interest

Dr. Vilim, Mrs. Ghazalova, Mrs. Petulova, Mrs. Horackova, Dr. Stepankova and Dr. Chaloupkova are employees, and Profs. Zbynek Prokop and Jiri Damborsky are co-founders of Enantis Ltd., which is the first biotechnology spin-off company of Masaryk University. The hyperstable FGF18-E4 (FGF18-STAB) is protected by the patent CZ 309 550.

Acknowledgments

Dr. Jan Vilim was supported by the grant Postdoc2MUNI (CZ.02.2.69/0.0/0.0/18_053/0016952). The authors would like to express gratitude to the Technological Agency of the Czech Republic (Retemed - TN02000122 and FW03010208) and the Czech Ministry of Education (ELIXIR CZ LM2023055 and eINFRA LM2018140) for the financial support. We would like to thank Dr. Barbara Hrdlickova for fruitful discussions about the cellular biology of FGF18.

Appendix A. Supporting information

Supplementary data associated with this article can be found in the online version at doi:10.1016/j.csbj.2023.10.009.

References

(1)Ornitz DM, Itoh N. New developments in the biology of fibroblast growth factors. No. November 2021 WIREs Mech Dis 2022. https://doi.org/10.1002/wsbm.1549.
(2)Turner N, Grose R. Fibroblast growth factor signalling: from development to cancer. Nat Rev Cancer 2010;10(2):116–29. https://doi.org/10.1038/nrc2780.

(3)Yun YR, Won JE, Jeon E, Lee S, Kang W, Jo H, et al. Fibroblast growth factors: biology, function, and application for tissue regeneration. J Tissue Eng 2010;1(1):1–18. https://doi.org/10.4061/2010/218142.
(4)Ornitz DM, Itoh N. The fibroblast growth factor signaling pathway. Wiley Interdiscip Rev Dev Biol 2015;4(3):215–66. https://doi.org/10.1002/wdev.176.
(5)Beenken A, Mohammadi M. The FGF family: biology, pathophysiology and therapy. Nat Rev Drug Discov 2009;8(3):235–53. https://doi.org/10.1038/nrd2792.
(6)Spielberger R, Stiff P, Bensinger W, Gentile T, Weisdorf D, Kewalramani T, et al. Palifermin for oral mucositis after intensive therapy for hematologic cancers. N Engl J Med 2004;351(25):2590–8. https://doi.org/10.1056/nejmoa040125.
(7)Liu Z, Lavine KJ, Hung IH, Ornitz DM. FGF18 is required for early chondrocyte proliferation, hypertrophy and vascular invasion of the growth plate. Dev Biol 2007;302 (1):80–91. https://doi.org/10.1016/j.ydbio.2006.08.071.
(8)Murugaiyan K, Amirthalingam S, Hwang NSY, Jayakumar R. Role of FGF-18 in bone regeneration. J Funct Biomater 2023;14(1). https://doi.org/10.3390/jfb14010036.
(9)Haque T, Nakada S, Hamdy RC. A review of FGF18: its expression, signaling pathways and possible functions during embryogenesis and post-natal development. Histol Histopathol 2007;22(1–3):97–105. https://doi.org/10.14670/HH-22.97.
(10)Yao X, zhang J, Jing X, Ye Y, Guo J, Sun K, et al. Fibroblast growth factor 18 exerts anti-osteoarthritic effects through PI3K-AKT signaling and mitochondrial fusion and fission. Pharmacol Res 2019;139:314–24. https://doi.org/10.1016/j.phrs.2018.09.026.
(11)Vos T, Allen C, Arora M, Barber RM, Brown A, Carter A, et al. Global, regional, and national incidence, prevalence, and years lived with disability for 310 diseases and injuries, 1990–2015: a systematic analysis for the global burden of disease study 2015. Lancet 2016;388(10053):1545–602. https://doi.org/10.1016/S0140-6736(16)31678-6.
(12)Long H, Liu Q, Yin H, Wang K, Diao N, Zhang Y, et al. Prevalence trends of site-specific osteoarthritis from 1990 to 2019: findings from the global burden of disease study 2019. Arthritis Rheumatol 2022;74(7):1172–83. https://doi.org/10.1002/art.42089.
(13)Hochberg MC, Guermazi A, Guehring H, Aydemir A, Wax S, Fleuranceau-Morel P, et al. Effect of intra-articular sprifermin vs placebo on femorotibial joint cartilage thickness in patients with osteoarthritis: the FORWARD randomized clinical trial. JAMA - J Am Med Assoc 2019;322(14):1360–70. https://doi.org/10.1001/jama.2019.14735.
(14)Dahlberg LE, Aydemir A, Muurahainen N, Gühring H, Fredberg Edebo H, Krarup-Jensen N, et al. A first-in-human, double-blind, randomised, placebo-controlled, dose ascending study of intra-articular RhFGF18 (Sprifermin) in patients with advanced knee osteoarthritis. Clin Exp Rheumatol 2016;34(3):445–50.
(15)Lohmander LS, Hellot S, Dreher D, Krantz EFW, Kruger DS, Guermazi A, et al. Intraarticular sprifermin (recombinant human fibroblast growth factor 18) in knee osteoarthritis: a randomized, double-blind, placebo-controlled trial. Arthritis Rheuma 2014;66(7):1820–31. https://doi.org/10.1002/art.38614.
(16)Buchtova M, Chaloupkova R, Zakrzewska M, Vesela I, Cela P, Barathova J, et al. Instability restricts signaling of multiple fibroblast growth factors. Cell Mol Life Sci 2015; 72(12):2445–59. https://doi.org/10.1007/s00018-015-1856-8.
(17)Dvorak P, Bednar D, Vanacek P, Balek L, Eiselleova L, Stepankova V, et al. Computer-assisted engineering of hyperstable fibroblast growth factor 2. Biotechnol Bioeng 2018; 115(4):850–62. https://doi.org/10.1002/bit.26531.
(18)Bednar D, Beerens K, Sebestova E, Bendl J, Khare S, Chaloupkova R, et al. FireProt: energy- and evolution-based computational design of thermostable multiple-point mutants. PLoS Comput Biol 2015;11(11). https://doi.org/10.1371/journal.pcbi.1004556.
(19)Ladel CH, Barbero L, Riva S, Guehring H. Tissue distribution of sprifermin (recombinant human fibroblast Growth Factor 18) in the rat following intravenous and intra-articular injection. Osteoarthr Cartil Open 2020;2(3). https://doi.org/10.1016/j.ocarto.2020.100068.
(20)Sayers EW, Agarwala R, Bolton EE, Brister JR, Canese K, Clark K, et al. Database resources of the national center for biotechnology information. Nucleic Acids Res 2019; 47(D1):D23–8. https://doi.org/10.1093/nar/gky1069.
(21)Li W, Godzik A. Cd-Hit: a fast program for clustering and comparing large sets of protein or nucleotide sequences. Bioinformatics 2006;22(13):1658–9. https://doi.org/10.1093/bioinformatics/btl158.
(22)Frickey T, Lupas A. CLANS: a java application for visualizing protein families based on pairwise similarity. Bioinformatics 2004;20(18):3702–4. https://doi.org/10.1093/bioinformatics/bth444.
(23)Edgar RC. MUSCLE: a multiple sequence alignment method with reduced time and space complexity. BMC Bioinforma 2004:5. https://doi.org/10.1186/1471-2105-5-113.
(24)Brown A, Adam LE, Blundell TL. The crystal structure of fibroblast growth factor 18 (FGF18. Protein Cell 2014;5(5):343–7. https://doi.org/10.1007/s13238-014-0033-4.
(25)Schymkowitz J, Borg J, Stricher F, Nys R, Rousseau F, Serrano L. The FoldX web server: an online force Field. Nucleic Acids Res 2005;33(SUPPL. 2):382–8. https://doi.org/10.1093/nar/gki387.
(26)Alford RF, Leaver-Fay A, Jeliazkov JR, O'Meara MJ, DiMaio FP, Park H, et al. The rosetta all-atom energy function for macromolecular modeling and design. J Chem Theory Comput 2017;13(6):3031–48. https://doi.org/10.1021/acs.jctc.7b00125.
(27)Kellogg EH, Leaver-Fay A, Baker D. Role of conformational sampling in computing mutation-induced changes in protein structure and stability. Proteins Struct Funct Bioinforma 2011;79(3):830–8. https://doi.org/10.1002/prot.22921.
(28)Ashkenazy H, Abadi S, Martz E, Chay O, Mayrose I, Pupko T, et al. ConSurf 2016: an improved methodology to estimate and visualize evolutionary conservation in macromolecules. Nucleic Acids Res 2016;44(W1):W344–50. https://doi.org/10.1093/NAR/GKW408.
(29)Koledova Z, Sumbal J, Rabata A, De La Bourdonnaye G, Chaloupkova R, Hrdlickova B, et al. Fibroblast growth factor 2 protein stability provides decreased dependence on heparin for induction of FGFR signaling and alters ERK signaling dynamics. Front Cell Dev Biol 2019:7. https://doi.org/10.3389/fcell.2019.00331.
(30)Ornitz DM, Xu J, Colvin JS, McEwen DG, MacArthur CA, Coulier F, et al. Receptor specificity of the fibroblast growth factor family. J Biol Chem 1996;271(25):15292–7. https://doi.org/10.1074/jbc.271.25.15292.
(31)Gasteiger E, Hoogland C, Gattiker A, Duvaud S, Wilkins MR, Appel RD, et al. Protein identification and analysis tools on the ExPASy server. Proteom Protoc Handb 2005: 571–607. https://doi.org/10.1385/1-59259-890-0:571.
(32)Kunka A, Marques SM, Havlasek M, Vasina M, Velatova N, Cengelova L, et al. Advancing enzyme's stability and catalytic efficiency through synergy of force-field calculations, evolutionary analysis, and machine learning. ACS Catal 2023:12506–18. https://doi.org/10.1021/acscatal.3c02575.
(33)Zhang X, Ibrahimi OA, Olsen SK, Umemori H, Mohammadi M, Ornitz DM. Receptor specificity of the fibroblast growth factor family: the complete mammalian FGF family. J Biol Chem 2006;281(23):15694–700. https://doi.org/10.1074/jbc.M601252200.
(34)Sennett ML, Meloni GR, Farran AJE, Guehring H, Mauck RL, Dodge GR. Sprifermin treatment enhances cartilage integration in an in vitro repair model. J Orthop Res 2018; 36(10):2648–56. https://doi.org/10.1002/jor.24048.
(35)Reker D, Kjelgaard-Petersen CF, Siebuhr AS, Michaelis M, Gigout A, Karsdal MA, et al. Sprifermin (RhFGF18) modulates extracellular matrix turnover in cartilage explants ex vivo. J Transl Med 2017;15(1):1–12. https://doi.org/10.1186/s12967-017-1356-8.
(36)Zhou Z, Song W, Zhang G, Zhan S, Cai Z, Yu W, et al. The recombinant human fibroblast growth factor-18 (Sprifermin) improves tendon-to-bone healing by promoting chondrogenesis in a rat rotator cuff repair model. J Shoulder Elb Surg 2022;31(8): 1617–27. https://doi.org/10.1016/j.jse.2022.01.137.
(37)Gigout A, Guehring H, Froemel D, Meurer A, Ladel C, Reker D, et al. Sprifermin (RhFGF18) enables proliferation of chondrocytes producing a hyaline cartilage matrix. Osteoarthr Cartil 2017;25(11):1858–67. https://doi.org/10.1016/j.joca.2017.08.004.
(38)Eckstein F, Hochberg MC, Guehring H, Moreau F, Ona V, Bihlet AR, et al. Long-term structural and symptomatic effects of intra-articular sprifermin in patients with knee osteoarthritis: 5-year results from the FORWARD study. Ann Rheum Dis 2021;80(8): 1062–9. https://doi.org/10.1136/annrheumdis-2020-219181.